J. Neely, J. Johnson, R. Bryne, R. T. Elliott, Structured optimization for parameter selection of frequency-watt grid support functions for wide-area damping, International Journal of Distributed Energy Resources and Smart Grids, vol. 11, no. 1, pp. 69-94, 2015.

STRUCTURED OPTIMIZATION FOR PARAMETER SELECTION OF FREQUENCY-WATT GRID SUPPORT FUNCTIONS FOR WIDE-AREA DAMPING

Jason Neely, Jay Johnson , Raymond Byrne, Ryan T. Elliott
Sandia National Laboratories
P.O. Box 5800 MS1033, Albuquerque, NM, USA 87185
Phone 1-505-845-7677, Fax 1-505-284-6078
E-mail: jneely@sandia.gov

Keywords: distributed energy resources, advanced grid functions, wide-area damping, inter-area oscillations, energy storage applications

ABSTRACT

Deployment of distributed renewable energy resources is increasing rapidly, which is leading to growing concerns over the impact of distributed power electronics energy converters on grid stability. In general, power electronic coupled systems do not provide frequency or voltage support through feedback compensation. This is leading to changes in utility interconnection requirements for distributed generation systems to provide voltage and frequency regulation ability through the use of newly developed advanced grid functions (AGFs). In this paper, the types of grid stability problems which can be mitigated by AGFs is expanded; in particular, it is demonstrated that the energy storage function which adjusts active power injection as a function of grid frequency, i.e., $P(f)$ or freq-watt, can provide damping control using local frequency information. Specifically, a structured optimization scheme is presented that is scalable to multi-node distributed damping applications. An algorithm computes optimal damping controller gains for distributed resources that use only local frequency feedback. The local control may be implemented using the freq-watt AGF recently defined by the International Electrotechnical Commission (IEC). The proposed approach is applicable to local and inter-area oscillation damping and could be valuable for utility operations centers to identify appropriate gains for installed systems that implement AGFs.

1 INTRODUCTION

Inverters that implement advanced grid functions (AGF) have the ability to assist with bulk system frequency problems, distribution-level voltage deviations, and provide additional protection and resiliency to the electric power system. These capabilities come at limited expense but can greatly increase the allowed penetration of photovoltaic and other renewable energy on the grid, reduce the size of ancillary services, and provide wide-area damping control. This paper introduces advanced DER grid requirements, identifies problems where advanced grid functions mitigate grid performance issues and discusses the need for AGF parameter optimization. In particular, this paper presents a scheme for optimally selecting parameters for frequency-watt functions to provide wide-area damping.

Many advanced grid functions are required in Europe and, more recently, in certain jurisdictions in the United States. Advanced grid functions in photovoltaic and energy storage inverters have been mandated in national grid codes for low and medium voltage interconnections in Italy, Spain, Germany, Austria, France, and other European nations [1]-[2]. These functions include low and high voltage ride through (L/HVRT), active power as a function of grid frequency, reactive power injection/absorption, and remote disconnection requirements [3].

In the United States, many jurisdictions are considering modifications to the DER interconnection requirements to utilize renewable energy and energy storage systems to support grid frequency and voltage. California has modified the Electric Rule 21 tariff [4] to include several AGF implementations in order to help CA utilities meet their aggressive renewable energy targets [5]-[6]. In January 2013, the California Public Utilities Commission (CPUC) convened the Smart Inverter Working Group (SIWG) composed of state agencies, utility engineers, national laboratories, manufacturers, trade associations, and advocacy groups to provide consensus AGF recommendations to the CPUC [7]. Pulling from the AGFs defined in the International Electrotechnical Commission (IEC) Technical Report 61850-90-7 [8] (Table 1.1), the SIWG recommendations were split into three-phases of deployment [7]:

- Phase 1 – autonomous functions, e.g., volt-var and frequency ride-through
- Phase 2 – communication functionality
- Phase 3 – advanced functions requiring communications, e.g., real power curtailment

In December 2014, the CPUC commissioners unanimously ratified the first phase of the SIWG recommendations, and it is expected that CA Rule 21 will require the second two SIWG phases in the near future.

Similarly, in Hawaii, high penetrations of renewable energy resources are challenging grid operators. This has led the three Hawaiian Electric Companies to issue a joint request that all DER on Oahu, Hawaii Island, Maui, Molokai, and Lanai be reprogrammed with *wider* frequency and voltage ride-through settings [9]. The

expanded ride-through settings are necessary so distributed generators do not trip when there are frequency or voltage excursions.

While certification and testing of advanced DER/inverter functionality is a major area of pre-standardization [10]-[12], selection of AGF parameters are also key to the successful deployment of the new technology. Just as the distributed controls of conventional generation must be harmonized to establish robust grid performance, the AGF parameters—e.g. curve shapes (deadbands and slopes), ramp rates, and delays—will become increasingly relevant as renewable penetration increases. In particular, unintended emergent behavior from untuned distributed controls can disrupt the grid as opposed to supporting it.

Table 1.1: IEC Technical Report 61850-90-7 Advanced Grid Functions

IEC 61850-90-7 Command/Function		General Category
INV1	Connect/disconnect	Immediate control functions
INV2	Adjust max generation level	
INV3	Adjust power factor	
INV4	Request active power (from storage)	
INV5	Signal for charge/discharge action	
VV11	Volt-Var mode 11 (watt priority)	Volt-var management modes
VV12	Volt-Var mode 12 (var priority)	
VV13	Volt-Var mode 13 (static mode)	
VV14	Volt-Var mode 14 (no var support)	
FW21	Set active power limits based on grid frequency	Frequency-Watt management modes
FW22	Set active power input/output limits based on grid frequency	
TV31	Dynamic reactive current support	
L/HVRT	Connect/disconnect settings for Low/High Voltage Ride-through (VRT)	"must disconnect" and "must remain connected" regions for freq. and voltage
L/HFRT*	Connect/disconnect settings for Low/High Frequency Ride-through (FRT)	
WP41	Feed-in power adjust power factor	Watt-triggered behavior modes
WP42	Feed-in power adjust power factor	
VW51	Adjust power output to smooth voltage	Voltage-Watt management modes
VW52	Adjust power input/output to smooth voltage	
TMP	Temperature mode behavior	
PS	Signal mode behavior	
DS91	Modify DER settings	Parameter setting and reporting
DS92	Log alarms and events/retrieve logs	
DS93	Status reporting	
DS94	Time synchronization	
* Low/High Frequency Ride Through is not included in IEC TR 61850-90-7 but is being considered by some jurisdictions, like California [7].		

The potential for disruption has been exemplified by the "50.2 Hz problem" in Europe, wherein a minor high frequency event would trip off gigawatts of distributed generation and lead to bulk system destabilization [13]. This will ultimately lead to expensive retrofits to more than 400,000 inverters to adjust the must-trip

L/HFRT settings and add new frequency-watt functionality which gradually reduces output power of DER as the frequency increases above 50.2 Hz [14] according to VDE AR-N 4105 [15]. To further mitigate this issue, PV systems in Germany rated for less than 30 kW must limit their power to 70% of nameplate capacity or disconnect when the Distribution System Operator (DSO) sends the DER a signal; larger systems must have the remote DSO disconnection capability [16]. For this reason, detailed analyses of the desired and unintended grid effects must be performed prior to selection or standardization of AGF parameters.

At a more local level, the AGF parameters can significantly impact distribution system operations and controls. EPRI has investigated selecting PV advanced inverter settings for volt-var, volt-watt, and power factor to optimize voltage drop, flicker, feeder line losses, overvoltages, or reduce regulator tap operations [17]. From their study, the optimal parameters were difficult to determine and slight variations in the settings yielded significantly different responses on the feeder. The best settings depended on interconnection location on the feeder, feeder load level and topology, and if there were other systems with AGFs on the feeder.

While European grid codes strictly define the parameters for AGFs, in California, there are default settings with wide ranges of adjustability for AGFs [18]-[20]; thereby allowing utilities to adjust the settings as necessary for their jurisdiction, but transferring the burden onto them to select settings which have not been standardized across the industry. To advise utility regulators in these jurisdictions, high-fidelity, analytical studies and field experiments are necessary to determine proper advanced DER settings.

Many researchers have investigated different advanced grid settings for grid support behaviors. For example, voltage control on distribution circuits (volt/var, fixed power factor, etc.) to increase the hosting capacity and maintain the circuit within the required voltage limits were studied in [20]-[25]. Similarly, Winter *et al*. investigated volt-watt functions for increasing the hosting capacity in Europe [25]. While wind [26]-[27] and energy storage systems [28] are commonly studied for frequency control, and optimal frequency control settings have been determined to mitigate high frequency disturbances and provide frequency regulation [29]-[33], they have not been investigated to provide wide area damping.

Poorly damped inter-area oscillatory modes have been identified as contributing to the August 10, 1996 blackout and system break-up of the Western North American Power System (wNAPS) [34]-[36] and to the August 14, 2003 blackout in the eastern interconnection in North America [36]. Power transfers are often limited by stability constraints, leading to concerns over low-damping conditions. Such problems have also been cited in the Nordic power system [37].

Use of the wide area measurement system (WAMS) as feedback to implement wide-area damping control has been investigated. In [38], the authors implement a wide-area damping control scheme based on a 180 MVAr static VAr compensator (SVC) using WAMS feedback. In [39],[40] the authors investigate the use of ener-

gy storage to dampen inter-area oscillations using local and remote frequency feedback, such as that from a WAMS system. In [41], the authors study and advocate the use of power modulation of the Pacific DC Intertie (PDCI), a high voltage DC transmission line, to dampen North-South inter-area oscillatory modes. In [42], the coordinated modulation of the PDCI and energy storage is considered.

This paper expands on previous work to develop a damping control scheme based on distributed active power modulation to provide wide-area damping control. The control is implemented using a specific IEC TR 61850-90-7 energy storage function which adjusts active power injection as a function of local grid frequency, and the function parameters are selected using an offline optimization that considers the grid dynamics as a whole. This approach has a number of benefits:

a. In contrast to the methods in [38]-[42], AGFs do not rely on the wide area measurement systems (WAMS) or require network access to real-time phasor measurement unit (PMU) data.
b. Reliance on *large N* distributed resources provides redundancy and thus robustness.
c. Implementation of the required functions is already underway by manufacturers and can make use of existing hardware.

To compute the freq-watt parameters, the damping control problem is first represented as a distributed optimal control problem with a quadratic cost function that considers local frequency error, inter-area frequency difference, and the normalized control effort. The gains are computed so as to minimize the cost function. In particular, the cost function formulation is customized to select only available feedback terms, and a numerical algorithm based on the Anderson-Moore search [43]-[46] is performed to find the optimal gains.

The remainder of this report is organized as follows. Characteristics of oscillatory modes and damping control using real power modulation are reviewed in Section 2 with a focus on the Western North American Power System (wNAPS). In Section 3, the small signal model is presented, and the distributed optimal control problem is formulated. In Section 4, a method is presented wherein the optimal control problem is solved numerically using the Anderson-Moore descent function. Two examples are presented in Section 5 including an application of the control to a minniWECC model of the wNAPS. Finally, conclusions are provided in Section 6.

2 BACKGROUND ON POWER SYSTEM OSCILLATIONS AND DAMPING CONTROL

This section introduces electromechanical oscillations in power systems, with particular focus on the wNAPS. Recent investigations into the use of real power modulation to improve system damping are then summarized.

2.1 Characteristics of Oscillatory Modes

Electrical mechanical oscillations in power systems contain both *local* and *inter area* modes. An *area* comprises a large complex of electrically close generators. Local oscillation modes pertain to electromechanical oscillations of a single generator or plant against the rest of the system while inter area modes pertain to oscillations between groups of generators in one area against groups of generators in a different area [48]. Modes are characterized by frequency, damping and shape. In the Western North American Power System (wNAPS), several characteristic inter area modes have been known to recur and exhibit a low damping condition. These modes include the following [48]:

- North-South A mode, nominally near 0.25 Hz
- North-South B mode, nominally near 0.4 Hz
- East-West mode, nominally near 0.5 Hz
- British Columbia (BC) mode, nominally near 0.6 Hz
- Montana mode, nominally near 0.8 Hz

2.2 Understanding and Visualizing Mode Shape

Small-signal stability is defined as "the ability of the power system to maintain synchronism under small disturbances" [50]. Even under normal operation, power systems experience ambient perturbations primarily as a result of random fluctuations in load. A disturbance is considered "small" if the response of the system can be sufficiently described by a linearized model. The underlying assumption is that about a particular operating point the behavior of a power system can be described by a set of ordinary differential equations of the form,

$$\dot{x}(t) = Ax(t) + B_e u_e(t) \tag{1}$$

where $x \in \mathbf{R}^n$ is the system state vector, which includes small-signal rotor angle and speed deviations among other quantities and $u_e \in \mathbf{R}^m$ is an exogenous input that may represent probing signals or other inputs designed to excite a system response [48]. The eigensolution of the system matrix *A* in (1) yields all of the information required to describe the modal properties of the system. The right eigenvector, called the "mode shape" vector, is a direct measure of the observability of a mode in the various states of the system. The magnitude and angle of the elements of the mode shape vector provide information about the relative oscillation amplitude and phase of a mode respectively. For analysis of inter-area modes, the elements of the mode shape vector corresponding to a common generator state, such as machine speed, are compared.

Classically, mode shape data is presented in polar form [51]. Each element of the mode shape vector corresponding to a common system state is plotted as a phasor. The phasor tails are arranged at the origin, creating a compass-like appearance.

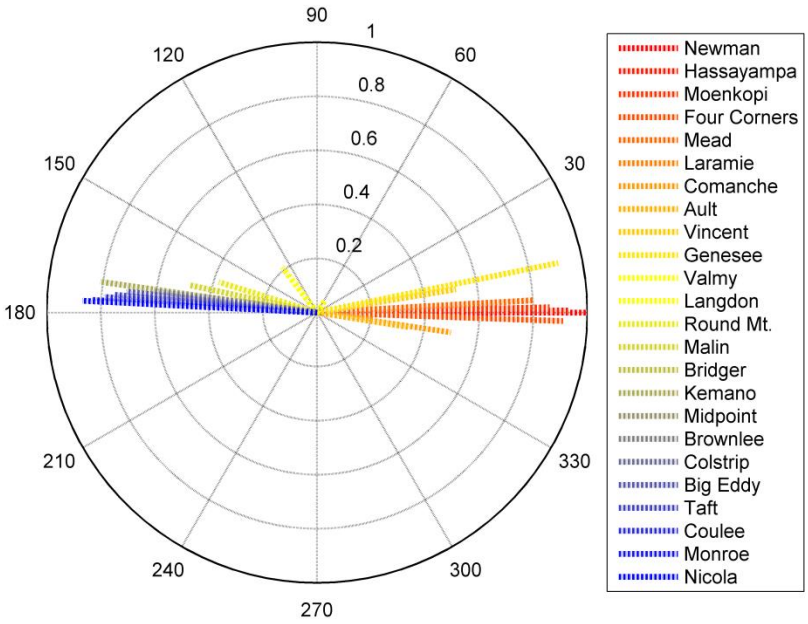

Figure 2.1: Compass plot example for mode shape data in Table 2.1.

An alternative method of presenting mode shape data is to generate a map and place the tail of each phasor at the location where the state was measured. To facilitate numerical comparison, the oscillation amplitude is normalized by the largest value, and the bus with the largest amplitude is used as the angle reference. Figure 2.2 displays a mode shape map example. Therein, the red and blue markers represent key generators or plants that are oscillating against one another in the specified mode, and marker diameter indicates the amplitude of oscillation.

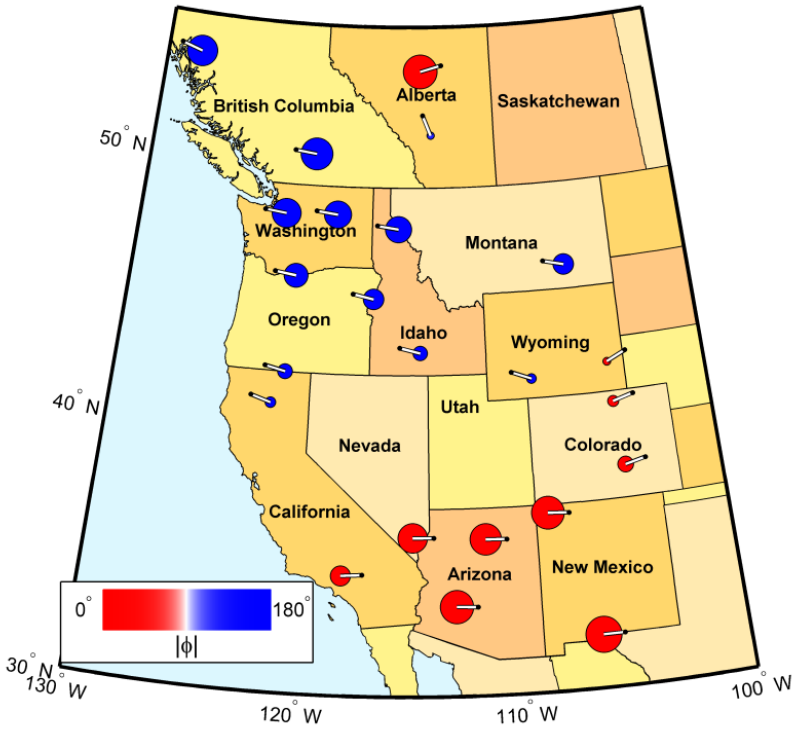

Figure 2.2: Representation of North-South B mode shape in the wNAPS.

The mode shape data for Figure 2.2 is presented in Table 2.1 below. The columns are arranged in order of descending oscillation amplitude.

Table 2.1: North-South B mode shape data for Figure 2.2

Bus	Amp.	Shape(*Deg.*)	Bus	Amp.	Shape(*Deg.*)
Newman	1.00	0.0	Nicola	0.87	177.1
Hassayampa	0.93	0.4	Monroe	0.83	176.8
Genesee	0.91	11.6	Kemano	0.81	171.9
Four Corners	0.91	−2.0	Coulee	0.79	175.8
Moenkopi	0.86	1.3	Taft	0.75	175.0
Mead	0.80	3.2	Big Eddy	0.71	173.7
Vincent	0.52	9.5	Brownlee	0.61	172.5
Comanche	0.50	−8.5	Colstrip	0.57	173.4
Ault	0.34	−9.1	Malin	0.48	167.9
Laramie	0.21	−6.8	Midpoint	0.43	172.1
Valmy	0.05	56.3	Round Mt.	0.38	162.8
			Bridger	0.29	171.6
			Langdon	0.21	127.5

3 OPTIMAL MULTI-NODE DISTRIBUTED DAMPING

In this section, the small-signal behavior of a power system is modeled as a linear system and modified to accommodate several distributed nodes participating in damping control. It is assumed that only local frequency measurements are available to each node.

3.1 Linearized Power System Model

To include the control action of distributed resources, the linearized power system model in (1) is expanded and represented as

$$\dot{x}(t) = Ax(t) + B_d u_d(t) + B_e u_e(t) \tag{2}$$

$$y(t) = Cx(t) \tag{3}$$

where $u_d \in \mathbf{R}^p$ is the input vector of real power injection intended to provide system damping and the output vector $y \in \mathbf{R}^h$ is a vector of generator speeds available for feedback.

As noted earlier, the stability of the system is described by the eigenvalues of the $n \times n$ matrix A, and the mode shape is encoded into the eigenvectors of A. Elements of the $n \times p$ matrix B_d would be determined by the location and interconnection of distributed damping control resources. The goal herein is to compute a $p \times h$ damping controller gain matrix K_d such that the eigenvalues of $A - B_d K_d C$ are further *left* in the complex plane, indicating improved damping. Furthermore, the selection of gain values should account for priorities concerning performance and control energy expended by the distributed resources. These priorities are represented using a performance index.

3.2 Definition of the Performance Index

The performance index, or *cost function*, is given as follows

$$J = \int_{t_0}^{\infty} \left(y^T Q y + u_d^T R u_d \right) d\tau \tag{4}$$

wherein the term $y^T Q y$ assigns a penalty for the state trajectory with $Q \succeq 0$, and $u_d^T R u_d$ penalizes the control energy with $R \succ 0$. For a damping control application $y^T Q y$ would be formulated to penalize frequency error (local and/or inter-area). The control design problem is thus to select the controller gain matrix K_d so as to minimize *J*.

The problem resembles the familiar *linear quadratic regulator* (LQR) problem wherein an optimal K_d is computed analytically through solution of the algebraic Riccati equation for full state feedback [49]. In this application however, since only the local system frequencies (and not the whole system state) may be used for

feedback at each distributed asset, a conventional linear quadratic regulator (LQR) solution may not be used. Thus, the LQR solution is not used directly to compute K_d; rather the solution is attained numerically. Herein, the solution is attained using a method based on the Anderson-Moore search algorithm.

4 NUMERICAL SOLUTION OF OPTIMAL CONTROL PROBLEM

To compute the optimal gains, the cost function formulation is augmented to assign additional cost to the undesired or unavailable feedback terms, and an iterative numerical structured control algorithm (SCA) based on the Anderson-Moore search [45]-[46] is performed to find the optimal gains. The Anderson-Moore algorithm is an algebraic algorithm that is particularly effective at handling linear systems with saddle points [43]-[44].

4.1 Augmented Performance Index and Optimization Problem

The damping controller inputs are partitioned into *p* areas/subsystems wherein

$$B_d u_d = \sum_{i=1}^{p} B_{d,i} u_{d,i} \tag{5}$$

$$u_{d,i} = K_{d,i} C_i, x, \; i \in \{1,2,...,p\} \tag{6}$$

In addition, the *R* matrix is assumed to be diagonal *R=diag(R_1, R_2, ..., R_p)*, and the control inputs are normalized such that $\tilde{u}_{d,i} = \sqrt{R_i} u_{d,i}$ where $u_{d,i}$ is the i^{th} element of u_d. In this case the control inputs, u_d, are provided by the frequency-watt function for energy storage systems using a linear droop controller defined in Figure 4.1 by points (F_1, GP_1) and (F_2, GP_2). In some cases, it may be necessary to establish a deadband around the nominal frequency to avoid excessive cycling of the energy storage system, as shown by the dashed freq-watt function in Figure 4.1. Herein, focus is placed on implementing a configuration without a deadband. The gain values appearing in the K_d matrix would thus be equated with the negative of the slope of the line in Figure 4.1, $-\dfrac{GP_1 - GP_2}{F_1 - F_2}$.

An additional cost term is formulated to penalize the use of unavailable or undesired feedback signals, and the term is added to the cost function, resulting in the expression

$$\tilde{J} = \int_{t_0}^{\infty} \left(y^T Q y + \tilde{u}_d^T \tilde{u}_d \right) d\tau + \left\| \tilde{K}_{d,i} \Gamma_i C_i x \right\|^2 \tag{7}$$

where $\Gamma_i \succeq 0$ is a diagonal matrix of weights that penalizes feedback of select signals.

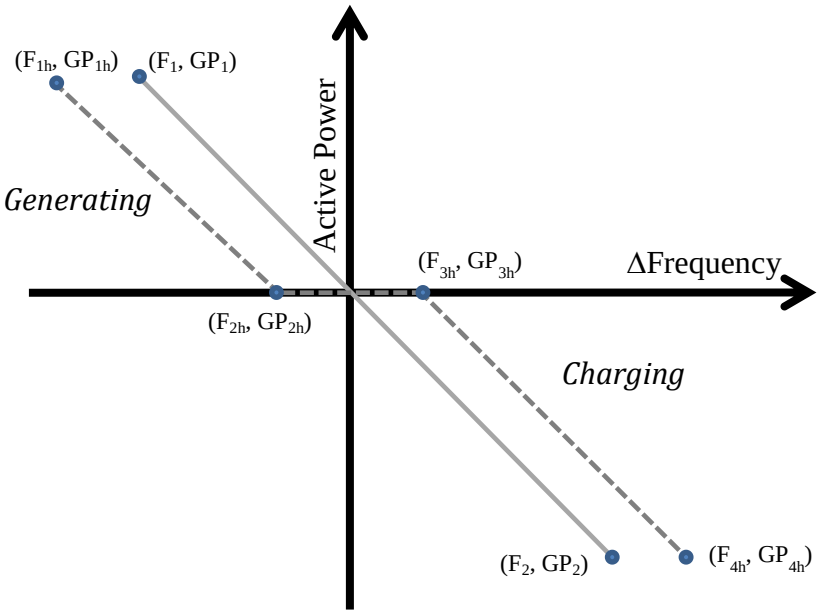

Figure 4.1: *The energy storage frequency-watt function with and without a deadband.*

The optimal damping control problem may be summarized as follows

$$\underset{K_d}{\text{minimize}} \quad \tilde{J}$$

subject to:

$$(1)\ \dot{x}(t) = \left(A - B_d \tilde{K}_d C\right)x(t)$$

$$(2)\ Q \succeq 0$$

$$(3)\ \Gamma_i \succeq 0$$

The gain matrix K_d is then determined through proper scaling of $\tilde{K}_d$.

4.2 Description of Anderson-Moore Search Algorithm

To solve the above optimization problem, a numerical algorithm is used to iteratively approach the solution. The algorithm requires the calculation of some intermediate quantities. In each iteration, $\tilde{K}_{d,i}$ values are updated and the system *A*-matrix is updated according to (8).

$$A_0 = A + \sum_{i=1}^{p} B_{d,i} \tilde{K}_{d,i} C_i \tag{8}$$

Likewise, the Q matrix is extended to include the control signal penalties according to (9).

$$Q_0 = Q + \sum_{i=1}^{p} \left(C_i^T \tilde{K}_{d,i}^T \tilde{K}_{d,i} C_i + C_i^T \Gamma_i^T \tilde{K}_{d,i}^T \tilde{K}_{d,i} \Gamma_i C_i \right) \tag{9}$$

In each iteration, a descent direction for the gain matrix is computed according to (10),

$$\Delta \tilde{K}_{d,i} = -\tilde{K}_{d,i} - B_{d,i}^T P X C_i^T \left(C_i X C_i^T + \Gamma_i \, C_i X C_i^T \Gamma_i^T \right)^{-1} \tag{10}$$

where X is the state covariance matrix. Herein, the gain matrix update uses the descent direction with a step size parameter $\alpha \in (0,1]$ to adjust the rate of convergence. These algorithm steps are summarized in Algorithm 1 below. In the next section, the algorithm is applied in the design of damping controllers for two example systems.

Algorithm 1: Structured Control Algorithm [45],[46]

1: Initialize the state Covariance X_0

2: Initialize K_d, and segment into p rows: $u_{d,i}$, $i \in \{1,2,...,p\}$

3: **while** change in gain is above tolerance $\Delta \left\| \tilde{K}_d \right\|_\infty > tol$, **do**

4: Compute A_0 using (8)

5: Solve $X_0 + X A_0^T + A_0 X = 0$ for X

6: Compute Q_0 using (9)

7: Solve $Q_0 + P A_0 + A_0^T P = 0$ for P

8: Compute new gain $\tilde{K}_{d,i} = \tilde{K}_{d,i} + \alpha \Delta \tilde{K}_{d,i}$ using (10)

9: **end while**

10: Compute $K_{d,i} = \dfrac{\tilde{K}_{d,i}}{\sqrt{R_i}}$, $\forall i \in \{1,2,...,p\}$

5 SIMULATION RESULTS

In this section, two control design examples are presented with simulation results. The first example considers a simplified three-area system with only primary speed

control and demonstrates the ability of the algorithm to prioritize control objectives. The second example demonstrates the approach on a minniWECC model of the wNAPS.

5.1 Simplified Three-Area Power System

Consider a simplified three area system wherein each area is modeled as a single generating unit with droop, speed governor and turbine. Each area model is consistent with the non-reheat steam turbine model described in [50]. The system is illustrated in Figure 5.1.

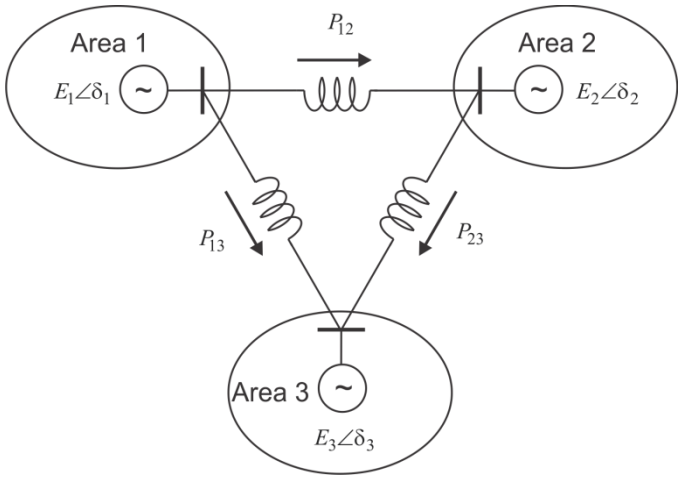

(a)

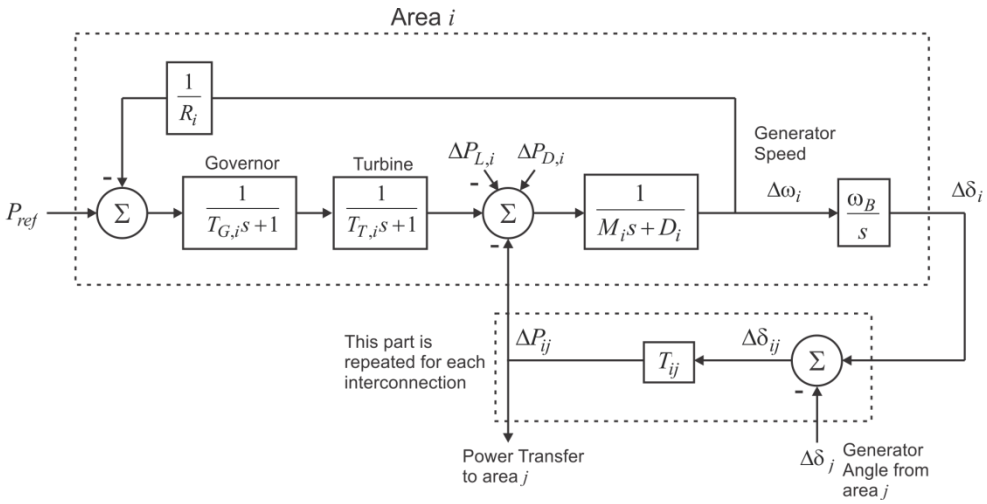

(b)

Figure 5.1: *Three area system showing (a) overview diagram of power system and (b) a system diagram for an individual area*

In each area, the generator speed is given as $\Delta\omega_i, i \in \{1,2,3\}$ (in per unit), the rotor angle is $\Delta\delta_i$ (radians), the inertia M_i (seconds) and damping coefficient D_i describe the rotor dynamics. The time constants associated with the speed governor and turbine are $T_{G,i}$ and $T_{T,i}$ respectively, and the droop coefficient is given by R_i. The synchronizing torque coefficients link an area *i* to an area *j*. The resulting system may be expressed using a state space model with $n = 12$: $x = \begin{bmatrix} \Delta x_1^T & \Delta x_2^T & \Delta x_3^T \end{bmatrix}^T$ where $\Delta x_i = \begin{bmatrix} \Delta\delta_i & \Delta\omega_i & \Delta Y_i & \Delta P_{m,i} \end{bmatrix}^T$ is the state vector for area *i*, with governor output ΔY_i and turbine mechanical power $\Delta P_{m,i}$. The base frequency of the system is given by ω_B. The damping powers are given by $u_d = \begin{bmatrix} \Delta P_{D,1} & \Delta P_{D,2} & \Delta P_{D,3} \end{bmatrix}^T$, and $u_e = \begin{bmatrix} \Delta P_{L,1} & \Delta P_{L,2} & \Delta P_{L,3} \end{bmatrix}^T$ are exogenous inputs representing changes in load-generation balance. System parameters are given in Table 5.2, and the output matrix is given in (11), but the remaining state space matrices are not shown for the sake of brevity.

$$y = \begin{bmatrix} \Delta\omega_1 \\ \Delta\omega_2 \\ \Delta\omega_3 \end{bmatrix} = Cx,\ C = \begin{bmatrix} 0 & 1 & 0 & 0 & 0 & 0 & 0 & 0 & 0 & 0 & 0 & 0 \\ 0 & 0 & 0 & 0 & 0 & 1 & 0 & 0 & 0 & 0 & 0 & 0 \\ 0 & 0 & 0 & 0 & 0 & 0 & 0 & 0 & 0 & 1 & 0 & 0 \end{bmatrix} \tag{11}$$

Table 5.1: Parameters for Three-Area System

Description	Parameter	Value (units)
Area inertias	$M_1,\ M_2,\ M_3$	6, 10, 5 (sec)
Area damping coefficients	$D_1,\ D_2,\ D_3$	0.4, 0.5, 0.3 (pu)
Governor Time Constant	$T_{G1},\ T_{G2},\ T_{G3}$	0.35, 0.30, 0.40 (sec)
Turbine Time Constant	$T_{T1},\ T_{T2}, T_{T3}$	0.5, 0.60, 0.60 (sec)
Droop Coeff.	$R_1,\ R_2,\ R_3$	0.065, 0.05, 0.072 (pu)
Synchronizing Torque Coeff.	$T_{12},\ T_{13},\ T_{23}$	0.0104, 0.0087, 0.0066 (pu)
Base Generator Speed	ω_B	120π (rad/sec)

In this example, the objective focuses on mitigating a poorly damped inter-area mode at a frequency of 0.35 Hz; this mode is primarily realized as an oscillation between areas 1 and 3. The penalty matrix may be formulated to isolate this mode as follows

$$y^T Q y = \left(\kappa_1\Delta\omega_1 + \kappa_2\Delta\omega_2 + \kappa_3\Delta\omega_3\right)^2 \tag{12}$$

where $\kappa_i \in \Re, i \in \{1,2,3\}$ are computed using terms in the right eigenvector.

The Γ_i matrices must be defined for each node location since only local feedback is used. These are defined as diagonal $h \times h$ matrices for the three areas as follows

$$\Gamma_1 = \eta \cdot diag([0 \quad 1 \quad 1]) \tag{13a}$$

$$\Gamma_2 = \eta \cdot diag([1 \quad 0 \quad 1]) \tag{13b}$$

$$\Gamma_3 = \eta \cdot diag([1 \quad 1 \quad 0]) \tag{13c}$$

where $\eta = 1000$ was found to work well in practice. Implementation of Algorithm 1 results in a gain matrix of

$$K_{d,local} = \begin{bmatrix} 1.5688 & 0 & 0 \\ 0 & 0.0896 & 0 \\ 0 & 0 & 1.6579 \end{bmatrix} \tag{14}$$

wherein the gain values used by the damping controller in areas 1, 2, and 3 appear in the first, second, and third rows respectively and are in per unit. For comparison, a "uniform gain" scenario is also considered wherein each area has the same local gain value of 1.5. Finally, a scenario is considered wherein each node has access to frequency information of all three areas through a network (i.e. such as WAMS). Using the same expression for (12) but using $\Gamma_1 = \Gamma_2 = \Gamma_3 = 0$, the algorithm provides the following gains

$$K_{d,netw} = \begin{bmatrix} 1.2709 & -0.0943 & -1.1788 \\ -0.0925 & 0.0202 & 0.0533 \\ -1.1606 & 0.0369 & 1.2750 \end{bmatrix} \tag{15}$$

wherein some portion of the $u_{d,i}$ applied in each area is based on feedback of remote signals.

The effect of the control may be illustrated through examination of the root loci of $A - B_d K_d C$ for each case. In the four examples given: (1) without damping control, (2) control using uniform gain, (3) control using local frequency feedback $K_{d,local}$, and (4) control using networked feedback $K_{d,netw}$ the root loci are shown in Figure 5.2 with the targeted mode at 0.35 Hz circled.

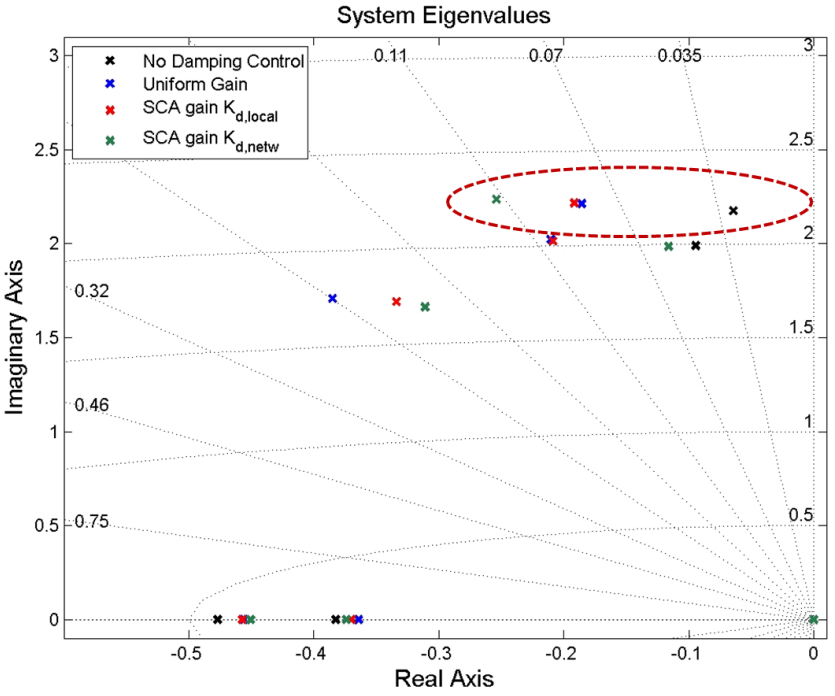

Figure 5.2: *Root Locus Comparison; 0.35 Hz mode is circled*

Damping at the targeted mode is improved from 2.96% to 8.62% using the SCA computed gains using local feedback and similarly to 8.35% using uniform gains. It is noted the uniform gain was selected to give similar damping at this mode.

The SCA computed gains using network feedback achieve 11.28% damping at the targeted mode. All three control schemes add damping to the 0.315 Hz mode. The uniform case adds the most damping to this case, but this mode is not the priority as defined by the cost function. The optimal networked solution adds the least to the 0.315 Hz mode as the control energy is better applied to the mode of interest.

The distinction in performance is further illustrated through simulation of the system. The system was simulated for 60 seconds with a 0.02 per unit load impulse applied to area 2. A linear combination of frequencies $\kappa_1 f_1 + \kappa_2 f_2 + \kappa_3 f_3$ is shown in Figure 5.3 to illustrate the mode behavior of interest. It is noted that the uniform gain case and $K_{d,local}$ case perform similarly at this mode. The $K_{d,netw}$ case actually has a slightly greater oscillation than in the $K_{d,local}$ case, but the overall system cost is the smallest with the $K_{d,netw}$ gains, 7.08×10^{-7} as compared with 4.06×10^{-6} with the $K_{d,local}$ gains. This is due primarily to the disparity in control energy. The control inputs u_d are shown in Figure 5.4. For the uniform

gain case, a disproportionately large level of control effort is seen in area 2. For the $K_{d,local}$ gains, the u_{d1} and u_{d3} control efforts are nearly equivalent to that seen in the uniform gain case; however, the u_{d2} control effort is greatly mitigated since this input has little controllability over the target mode. The network gain case with $K_{d,netw}$ shows a clear reduction in control energy over the other two cases; this is because the u_{d1} and u_{d3} controls are 180° out of phase, thus improving the inter-area damping torque with less control energy.

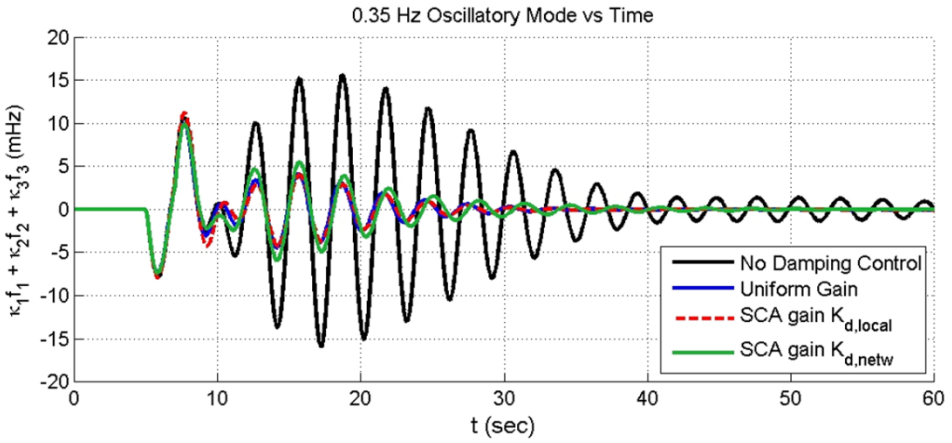

Figure 5.3: Simulation of three-area system with impulse in area 1 showing oscillation of 0.35 Hz mode

Given this simulation result, the cost associated with the control effort $\int\left(u_d^T u_d\right)dt$ is 1.055×10^{-5} for the uniform gain case, but 3.74×10^{-6} for the SCA local feedback case; this is 64.5% less cost while accomplishing slightly better damping at the target mode. For the SCA gains with network feedback, the cost of the control effort is 3.47×10^{-7} which is a more than 90% reduction in cost while accomplishing a 30.9% improvement in the added damping over the same.

The time domain response and thus the system cost will depend greatly on the disturbance input as well as the control gains. Not all scenarios will demonstrate such a large benefit for the proposed control. However, it is demonstrated that the algorithm can compute gains that result in a more optimal allocation of control energy. This would be useful for utilities that wish to realize prioritized wide area damping control given limited resources, i.e. PV curtailment or energy storage.

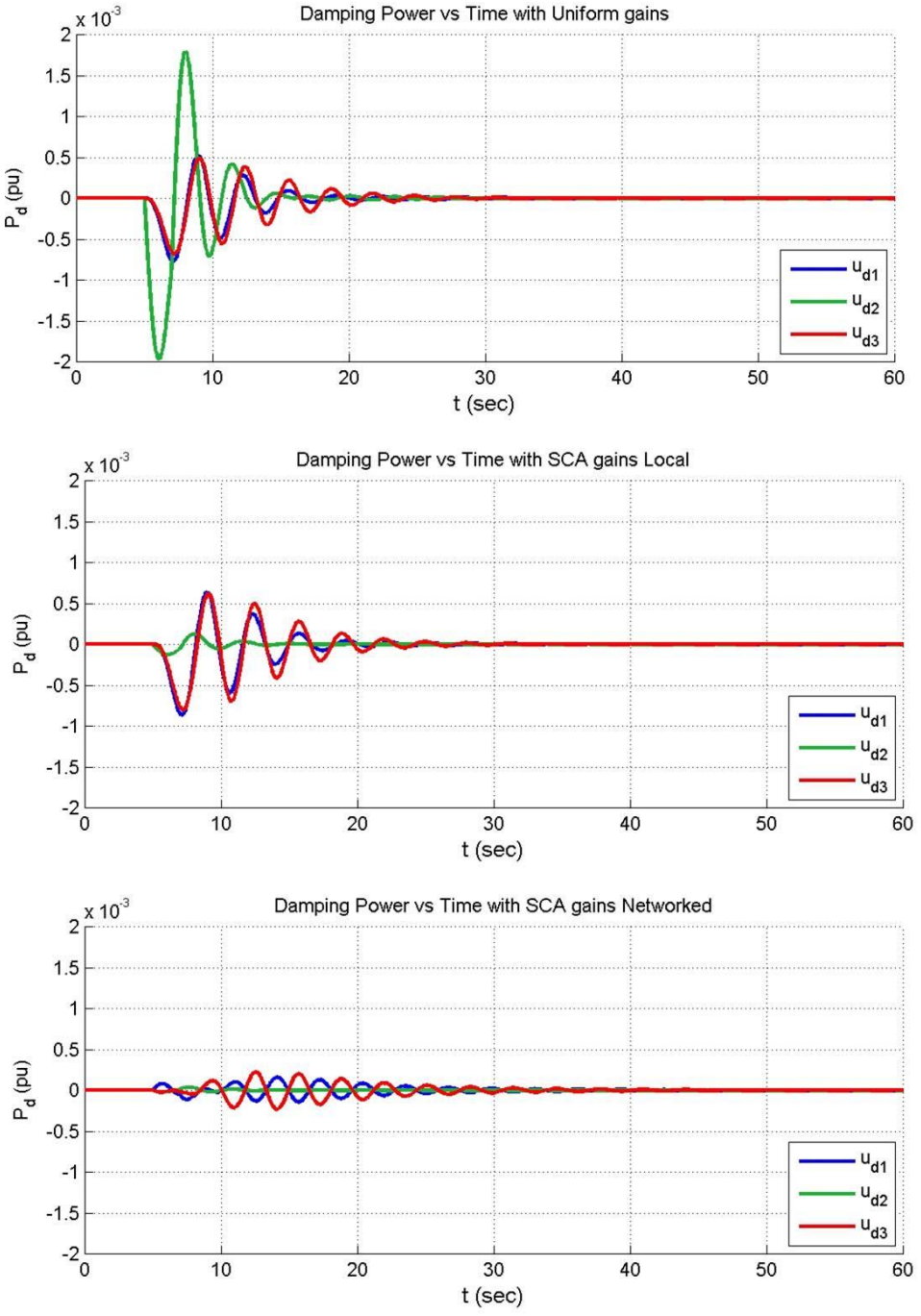

Figure 5.4: *Simulation of three-area system with impulse in area 1showing per unit damping powers with each meth*

5.2 Damping Control Design in the wNAPS using the minniWECC

This section presents simulation results for a reduced order model of the Western North American Power System (wNAPS). The model, referred to as the minniWECC, was developed by Dan Trudnowksi and John Undrill [41] using the MATLAB Power System Toolbox (PST) simulation framework. The PST was originally developed by Prof. Joe Chow and Kwok Cheung in the early 1990's [52]. It was further marketed and developed by Graham Rogers, and is currently available from Luigi Vanfretti's web site [53]. The minniWECC contains 34 generators, 122 buses, 171 lines and transformers, 19 load buses, and two DC lines. Highly detailed generator models are used in the model. The minniWECC network is illustrated in Figure 5.5.

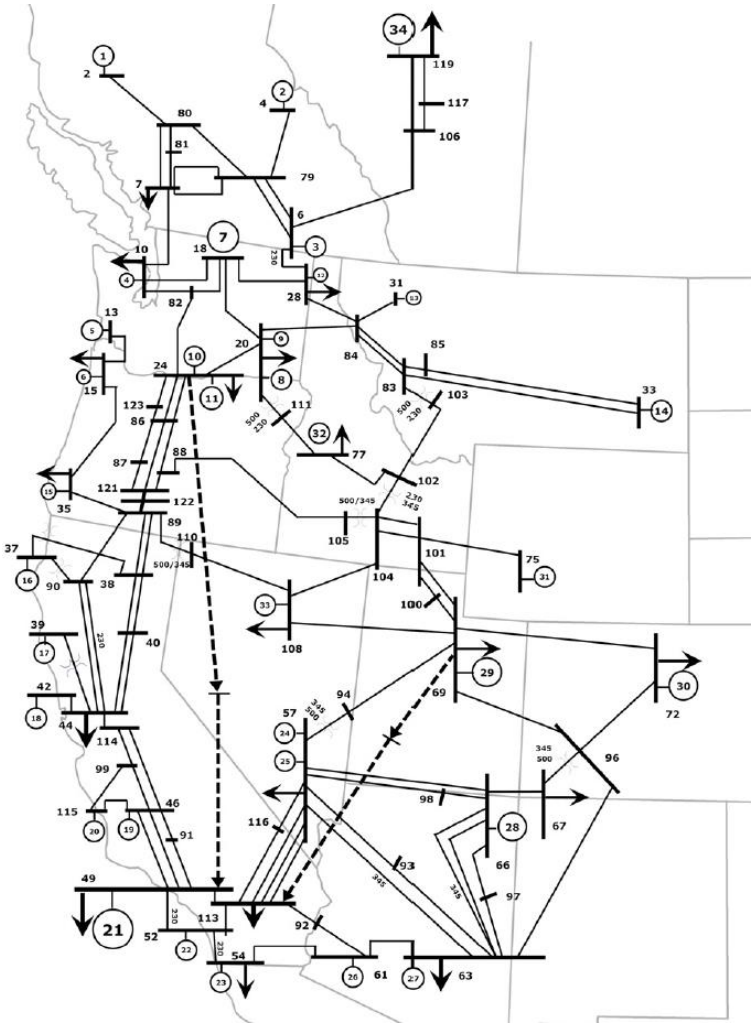

Figure 5.5: *Illustration of minniWECC reduced order model, reproduced from [40]*

For this analysis, a linearized model derived for the nonlinear minniWECC model was employed. The linearized model is obtained by perturbing the nonlinear system, using the **svm_mgen** routine in the Power Systems Toolbox. The result is state-space model with *A*, *B*, and *C* matrices that are used directly for defining (3) and (4) in the small-signal model.

Assuming a damping control resource may be installed at each of the *N* buses hosting a generator in the minniWECC model, a cost function is formulated to penalize East-West mode oscillations, and given as

$$y^T Q y = \left(\sum_{i=1}^{N} \kappa_i \Delta\omega_i \right)^2 \tag{16}$$

where the $\kappa_i, i \in \{1,2,...,N\}$ terms are determined similarly from the right eigen vector as noted in the three area example. Algorithm 1 was utilized to compute the optimal gains based on local frequency feedback. The results are shown in Figure 5.6. Therein, one notes the three largest damping gains are seen at generators 21 (southern California), 29, and 30 (Colorado).

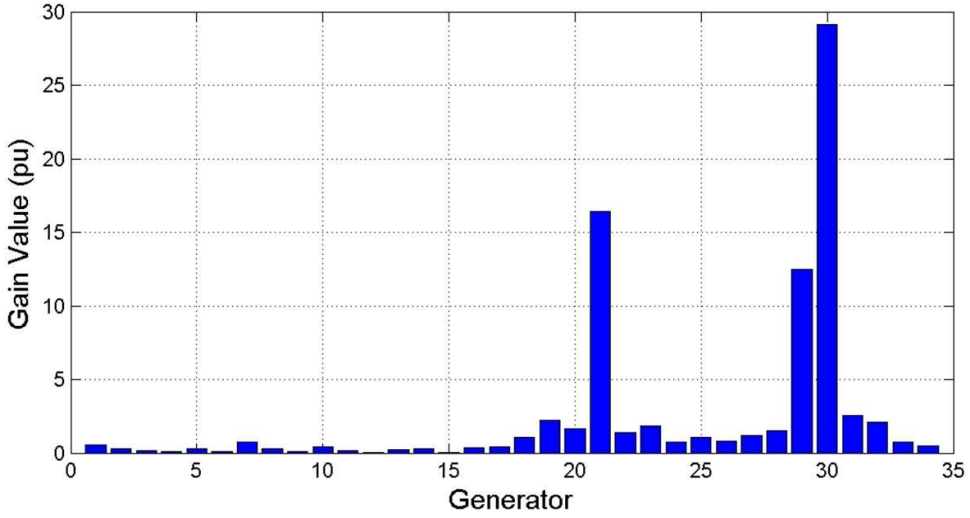

Figure 5.6: *Damping K gains determined by Algorithm 1 for the minniWECC*

The root locus is shown in Figure 5.7 wherein several electromechanical modes are illustrated. The cost function (16) was configured to penalize the East-West mode which is nominally at 0.50 Hz. Significant improvement is seen in several of the modes, including higher frequency (local) modes; however, most of the benefit is realized in the mode of interest, and no eigenvalues are seen to move to the right. Thus, the algorithm is successful in realizing the control objective.

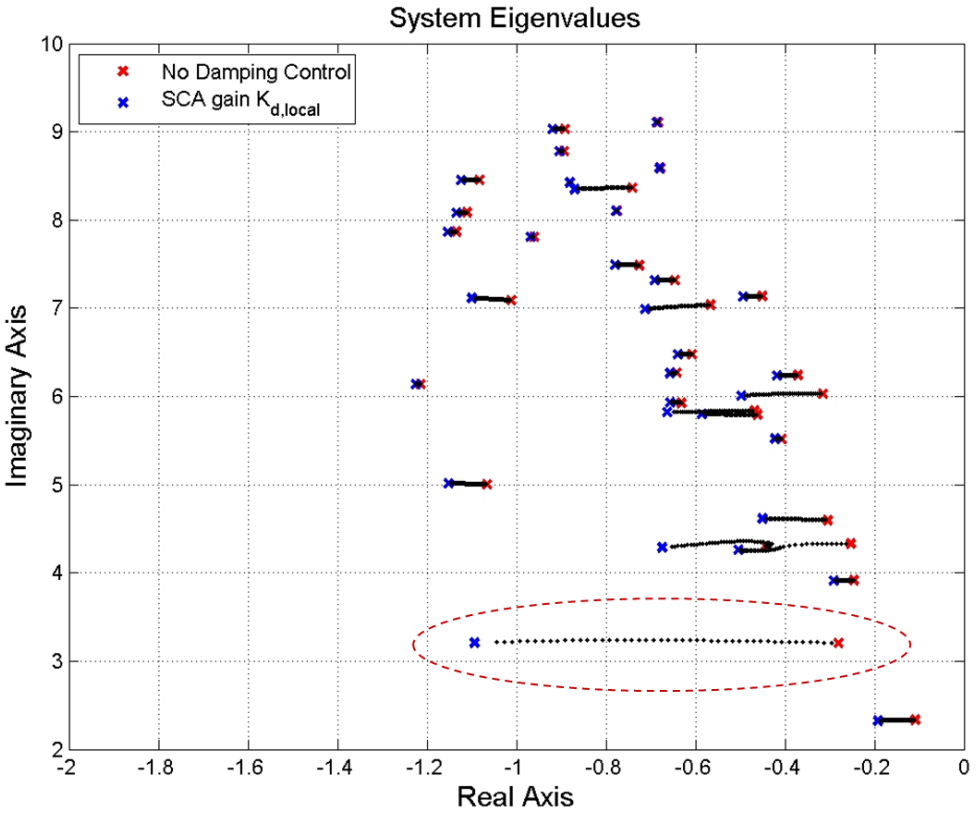

Figure 5.7: *MinniWECC eigenvalues due to damping K gains; East-West mode is circled*

6 CONCLUSIONS AND FUTURE WORK

Advanced grid function (AGF) requirements for renewable energy and energy storage systems are being added to many jurisdictions in Europe and the United States to provide grid operators additional control capabilities. These functions can be programmed to support grid frequency and voltage, and assist during grid disturbances. Many of the functions have been standardized in grid codes and IEC TR 61850-90-7, but the parameters for specific grid needs are still not well understood. While the optimal parameters are likely to change based on the grid topology and objectives, it may be possible to standardize methods for determining parameters which can achieve specific goals.

Studies that compare or optimize AGF settings cannot be comprehensive for all situations because of the wide range of distribution/transmission system variations, PV installation locations, and simulated PV penetration levels, so in many cases code and standards-making bodies rely on industry experts and anecdotal experi-

ence to select default AGF values. However, as the body of knowledge from simulations and field experience increases, better AGF parameters can be required by grid codes and programmed into DER.

This manuscript focused on the optimal allocation of control energy via selection of AGF parameters to assist transmission operators in preventing inter-area oscillations. Poorly damped oscillatory modes have caused multiple blackouts in the United States, but optimal distributed active power modulation can improve wide-area damping and prevent such events in the future. Here, the frequency-watt function applied to energy storage systems (ESSs) was optimized using a numerical algorithm based on the Anderson-Moore search and a quadratic cost function that considered local frequency error, inter-area frequency difference, and the normalized control effort. In particular, the flexibility of the approach allows for specific oscillatory modes to be prioritized ensuring optimal use of the control energy.

Simulation of a three-area system and a model of the Western North American Power System (called minniWECC) demonstrated system damping was improved using the optimal local ESS control gains. The autonomous, local control alone is not as effective as using wide-area measurement system (WAMS) feedback, but this method has a distinct advantage in that it does not rely on WAMS network access to real-time PMU data. Therefore, this method is more resilient to communication failures by eliminating the need for external data, and it is more robust since it utilizes distributed redundant resources.

This work could be expanded in the future by providing wide-area oscillation damping using curtailed PV systems with generation headroom or reactive power (e.g., [54]). Therefore, future wide-area damping optimization should consider other DER types and advanced grid functions such as volt-var.

7 ACKNOWLEDGMENT

The authors would like to thank the Department of Energy (DOE) Energy Storage Program (Dr. Imre Gyuk), the DOE Transmission Reliability Program (Mr. Phil Overholt), DOE Office of Electricity (Mr. Dan Ton), and the Bonneville Power Administration Technology Innovation Program (Dr. Jisun Kim and Dr. Dmitry Kosterev) for funding this research. In addition, this material is based in part upon work supported by the U.S. Department of Energy SunShot program under Award Number 29094.

Additionally, the authors would like to thank Matthew Reno and Abraham Ellis for technical reviews of the manuscript and Professor Dan Trudnowski for his support in using the minniWECC model.

Sandia National Laboratories is a multi-program laboratory managed and operated by Sandia Corporation, a wholly owned subsidiary of Lockheed Martin Corpora-

tion, for the U.S. Department of Energy‘s National Nuclear Security Administration, under contract DE-AC04-94AL85000.

8 REFERENCES

[1] R. Bründlinger *Grid Codes in Europe for Low and Medium Voltage*. 6th International Conference on Integration of Renewable and Distributed Energy Resources, Kyoto, Japan, 18 November, 2014.

[2] R. Bründlinger “European Codes & Guidelines for the Application of Advanced Grid Support Functions of Inverters”, Sandia/EPRI PV Systems Symposium - PV Distribution System Modeling Workshop, Santa Clara, CA, USA, 2014.

[3] J. Johnson, S. Gonzalez, A. Ellis, “Sandia DER Interoperability Test Protocols; Relationship to Grid Codes and Standards”, IEEE International Conference on Standards for Smart Grid Ecosystems, Bangalore, India. 6-7 Mar, 2014.

[4] California Public Utilities Commission, Electric Rule 21, Interconnection Proceeding Rulemaking 11-09-011, updated Dec. 18, 2014.

[5] T. Hsu, Los Angeles Times, “Gov. Brown pushes 12-gigawatt clean-power goal,” July 26, 2011.

[6] J.F. Wiedman, et al., Interstate Renewable Energy Council, “12,000 MW of Renewable Distributed Generation by 2020,” July 2012.

[7] California Public Utilities Commission, “Recommendations for Updating the Technical Requirements for Inverters in Distributed Energy Resources, Smart Inverter Working Group Recommendations,” Filed 7 February 2014.

[8] IEC Technical Report IEC 61850-90-7, “Communication networks and systems for power utility automation–Part 90-7: Object models for power converters in distributed energy resources (DER) systems,” Edition 1.0, Feb 2013.

[9] D. Ishimura, “Request to Implement Expanded Inverter Ride-Through Settings”, Memorandum to Inverter manufacturers from Hawaiian Electric Companies, 24 Nov., 2014.

[10] J. Johnson, R. Bründlinger, C. Urrego, R. Alonso, “Collaborative Development Of Automated Advanced Interoperability Certification Test Protocols For PV Smart Grid Integration,” EU PVSEC, Amsterdam, Netherlands, 22-26 Sept, 2014.

[11] J. Johnson, B. Fox, “Automating the Sandia Advanced Interoperability Test Protocols,” 40th IEEE PVSC, Denver, CO, 8-13 June, 2014.

[12] J. Johnson S. Gonzalez, M.E. Ralph, A. Ellis, and R. Broderick, "Test Protocols for Advanced Inverter Interoperability Functions," Sandia Technical Report SAND2013- 9880 and SAND2013-9875, Nov. 2013.

[13] J. C. Boemer, *et al* "Overview of German Grid Issues and Retrofit of Photovoltaic Power Plants in Germany for the Prevention of Frequency Stability Problems in Abnormal System Conditions of the ENTSO-E Region Continental Europe," 1st international workshop on integration of solar power into power systems, Denmark, October 2011.

[14] M. Sieg, "Germany retrofits 200,000 PV installations to meet 50 Hz requirement," PV Magazine, 28 Aug. 2014.

[15] VDE Application Guide VDE-AR-N 4105: Generators in the low voltage distribution network. Application guide for generating plants' connection to and parallel operation with the low-voltage network, 1/08/2010.

[16] J. von Appen, M. Braun, T. Stetz, K. Diwold, D. Geibel, "Time in the Sun: The Challenge of High PV Penetration in the German Electric Grid," Power and Energy Magazine, IEEE , vol.11, no.2, pp.55,64, March-April 2013.

[17] J. Smith, M. Rylander, H. Li, "Determining Recommended Settings for Smart Inverters," PV Distribution System Modeling Workshop, Santa Clara, CA, May 7, 2014.

[18] J.T. Sullivan, CPUC Rulemaking 11-09-011 Agenda ID #13460, 13 November, 2014, Approved Dec. 2014.

[19] IEEE Standard 1547a, "IEEE Standard for Interconnecting Distributed Resources with Electric Power Systems - Amendment 1", 2014.

[20] J.W. Smith, W. Sunderman, R. Dugan, B. Seal, "Smart inverter volt/var control functions for high penetration of PV on distribution systems," Power Systems Conference and Exposition (PSCE), 2011 IEEE/PES , vol., no., pp.1,6, 20-23 March 2011.

[21] M. Braun, T. Stetz, T. Reimann, B. Valov, and G. Arnold, "Optimal Reactive Power Supply in Distribution Networks–Technological and Economic Assessment for PV-Systems," in 24th European Photovoltaic Solar Energy Conference, Hamburg, Germany, 2009.

[22] T. Stetz, W. Yan, and M. Braun, "Voltage Control in Distribution Systems with High Level PV-Penetration," in 25th European PV Solar Energy Conference, Valencia, Spain, 2010.

[23] J. Seuss, M.J.Reno, R.J. Broderick, R.G. Harley, "Evaluation of reactive power control capabilities of residential PV in an unbalanced distribution feeder," 2014 IEEE 40th Photovoltaic Specialist Conference (PVSC), pp. 2094-2099, 8-13 June 2014.

[24] M.J. Reno, K. Coogan, S, Grijalva, R.J. Broderick, J.E. Quiroz, "PV interconnection risk analysis through distribution system impact signatures and feeder zones," 2014 IEEE PES General Meeting | Conference & Exposition, pp.1-5, 27-31 July 2014.

[25] C. Winter, R. Schwalbe, M. Heidl, W. Pruggler, "Harnessing PV inverter controls for increased hosting capacities of smart low voltage grids: Recent results from Austrian research and demonstration projects." 4th International Workshop on Integration of Solar Power into Power Systems, Berlin, Germany, 10-11 Nov, 2014.

[26] H. Bevrani, A. Ghosh, G. Ledwich, "Renewable energy sources and frequency regulation: survey and new perspectives, " Renewable Power Generation, IET, vol.4, no.5, pp.438-457, September 2010.

[27] J. Aho, et al., "Tutorial of Wind Turbine Control for Supporting Grid Frequency through Active Power Control," 2012 American ControlConference, Montreal, Canada, June 27-29, 2012.

[28] A. Oudalov; D. Chartouni, C. Ohler, "Optimizing a Battery Energy Storage System for Primary Frequency Control," IEEE Transactions on Power Systems, vol.22, no.3, pp.1259-1266, Aug. 2007.

[29] A. Hoke, D. Maksimovic, "Active power control of photovoltaic power systems," 2013 1st IEEE Conference on Technologies for Sustainability (SusTech), pp.70-77, 1-2 Aug. 2013.

[30] M. Datta, T. Senjyu, A. Yona, T. Funabashi, Chul-Hwan Kim, "A Frequency-Control Approach by Photovoltaic Generator in a PV–Diesel Hybrid Power System," IEEE Transactions on Energy Conversion, vol. 26, no. 2, pp. 559-571, June 2011.

[31] P.P. Zarina, S. Mishra, P.C. Sekhar, Exploring frequency control capability of a PV system in a hybrid PV-rotating machine-without storage system, International Journal of Electrical Power & Energy Systems, vol. 60, September 2014, pp. 258-267.

[32] H. Xin, Y. Liu, Z. Wang, D. Gan, T. Yang, "A New Frequency Regulation Strategy for Photovoltaic Systems Without Energy Storage," IEEE Transactions on Sustainable Energy, vol. 4, no. 4, pp.985,993, Oct. 2013.

[33] N. Kakimoto, S. Takayama, H. Satoh, K. Nakamura, "Power Modulation of Photovoltaic Generator for Frequency Control of Power System," IEEE Transactions on Energy Conversion, vol. 24, no. 4, pp.943-949, Dec. 2009.

[34] D. Kosterev, C. Taylor, and W. Mittelstadt, "Model Validation for the August 10, 1996 WSCC system outage," IEEE Trans on Power Systems, vol. 14, no. 3, August 1999.

[35] J. F. Hauer and J. E. Dagle, “Review of Recent Reliability Issues and System Events,” PNNL technical report PNNL-13150, prepared for the U.S. Department of Energy Transmission Reliability Program by the Consortium for Electric Reliability Solutions (CERTS), December 1999.

[36] J.Y. Cai, Z. Huang, J. Hauer, K. Martin, "Current Status and Experience of WAMS Implementation in North America," 2005 IEEE/PES Transmission and Distribution Conference and Exhibition: Asia and Pacific, pp.1-7, 2005.

[37] P. Korba, K. Uhlen, "Wide-area monitoring of electromechanical oscillations in the nordic power system: practical experience," Generation, Transmission & Distribution, vol. 4, no. 10, pp.1116-1126, October 2010.

[38] K. Uhlen, L. Vanfretti, M.M. de Oliveira, A.B. Leirbukt, V.H. Aarstrand, J.O. Gjerde, "Wide-Area Power Oscillation Damper implementation and testing in the Norwegian transmission network," 2012 IEEE Power and Energy Society General Meeting, pp.1-7, 22-26 July 2012.

[39] J. Neely, R. Byrne, R. Elliott, C. Silva-Monroy, D. Schoenwald, D. Trudnowski, and M. Donnelly, “Damping of inter-area oscillations using energy storage,” 2013 IEEE Power and Energy Society General Meeting (PES), July 2013.

[40] R.H. Byrne, D.J. Trudnowski, J.C. Neely, R.T. Elliott, D.A. Schoenwald, M.K. Donnelly, "Optimal locations for energy storage damping systems in the Western North American interconnect," 2014 IEEE PES General Meeting | Conference & Exposition, pp.1-5, 27-31 July 2014

[41] D. Trudnowski, D. Kosterev, J. Undrill, "PDCI damping control analysis for the western North American power system," 2013 IEEE Power and Energy Society General Meeting (PES), pp.1-5, 21-25 July 2013.

[42] J. Neely, R. Elliott, R. Byrne, D. Schoenwald, D. Trudnowski; “The Benefits of Energy Storage Combined with HVDC Transmission Power Modulation for Mitigating Inter-Area Oscillations”, Electrical Energy Storage Applications and Technologies (EESAT) Conference, San Diego, CA, October, 2013.

[43] G. Anderson and G. Moore, “A linear algebraic procedure for solving linear perfect foresight models,” Economics Letters, vol. 17, 1985.

[44] G. Anderson, “A reliable and computationally efficient algorithm for imposing the saddle point property in dynamic models,” Journal of Economic Dynamics and Control, vol. 34, pp. 472–489, 2010.

[45] H.T. Toivonen, P.M. Mäkilä, A descent Anderson-Moore algorithm for optimal decentralized control, Automatica, Volume 21, Issue 6, November 1985, Pages 743-744.

[46] J. Wolfe and D. Chichka, “An efficient design algorithm for optimal fixed structure control,” Proceedings of the 36th IEEE Conference on Decision and Control, vol. 3, pp. 2625–2627, December 1997.

[47] J. Undrill, “Investigation of asymptotic stability of low frequency oscillations,” Technical Report to Bonneville Power Administration, Portland, OR, 2010.

[48] D.Trudnowski and J. Pierre, “Signal processing methods for estimating small-signal dynamic properties from measured responses,” in Chapter 1 of Inter-area Oscillations in Power Systems; ed. A. R. Messina; Springer; New York; 2009.

[49] P. Dorato, C. Abdallah, and V. Cerone, Linear Quadratic Control an Introduction. Malabar, Fl: Krieger Publishing Company, second ed., 2000.

[50] P. Kundur, Power System Stability and Control. New York. Saddle River, NJ; Prentice Hall, 1996.

[51] G. Rogers, *Power System Oscillations*. Boston: Kluwer Academic Publishers, 2000.

[52] J. H. Chow, and K. W. Cheung, “A toolbox for power system dynamics and control engineering education and research,” IEEE Transactions on Power Systems, vol. 7, no. 4, pp. 1559-1564, 1992.

[53] L. Vanfretti. "Power System Toolbox Webpage," URL: http://www.eps.ee.kth.se/personal/luigiv/pst/Power_System_Toolbox_Webpage/PST.html.

[54] J. F. Hauer, "Reactive Power Control as a Means for Enhanced Interarea Damping in the Western U. S. Power System - A Frequency-Domain Perspective Considering Robustness Needs," *Application of Static Var Systems for System Dynamic Performance*, IEEE Publication 87TH0187-5-PWR, pp. 79-92, 1987.